NANO · MICRO small
www.small-journal.com

Fabrication of Nanoreaction Clusters with Dual-Functionalized Protein Cage Nanobuilding Blocks

*Hyukjun Choi, Bongseo Choi, Gwang Joong Kim, Han-ul Kim, Hansol Kim, Hyun Suk Jung, and Sebyung Kang**

Fabrication of functional nanostructures is a prominent issue in nanotechnology, because they often exhibit unique properties that are different from the individual building blocks. Protein cage nanoparticles are attractive nanobuilding blocks for constructing nanostructures due to their well-defined symmetric spherical structures, polyvalent nature, and functional plasticity. Here, a lumazine synthase protein cage nanoparticle is genetically modified to be used as a template to generate functional nanobuilding blocks and covalently display enzymes (β-lactamase) and protein ligands (FKBP12/FRB) on its surface, making dual-functional nanobuilding blocks. Nanoreaction clusters are subsequently created by ligand-mediated alternate deposition of two complementary building blocks using layer-by-layer (LbL) assemblies. 3D nanoreaction clusters provide enhanced enzymatic activity compared with monolayered building block arrays. The approaches described here may provide new opportunities for fabricating functional nanostructures and nanoreaction clusters, leading to the development of new protein nanoparticle-based nanostructured biosensor devices.

1. Introduction

Achieving fine organization and fabrication of functional nano- or biomaterials is one of the important issues in nanotechnology since collective properties generated by nanostructured materials frequently differ from the individual starting materials.[1] Various types of nanomaterials including organic and/or inorganic nanoparticles have been developed as nanoscale building blocks, and the fabrication processes incorporate highly active nanoscale components into simple and miniaturized devices that are applied to the development of a variety of nanosensors, catalysts, and nanoelectric devices.[2] Among the many nanoscale building blocks, protein cage nanoparticles are attractive candidates for use as nanobuilding blocks due to their uniform size, polyvalency, functional flexibility, and biocompatibility. The atomic structures of protein cage nanoparticles allow us to impart various functional ligands to them through both genetic and chemical modifications at specific locations. Such site-directed modifications and their highly symmetric nature enable us to construct functional nanobuilding blocks and high-ordered functional nanostructures. There are many approaches that utilize protein cage nanoparticles as building blocks for fabrication of high-ordered nanostructure, such as layer-by-layer (LbL) deposition, ordered planar arrays, and 3D lattice structures.[3] One approach is to use additional molecules which mediate interactions among protein cages nanoparticles. Modulating electrostatic interactions between dendrimers and protein cage nanoparticles, such as P22, cowpea chlorotic mottle virus (CCMV), and ferritin, were used to successfully construct high-ordered structures.[3l,m,][4] In addition to dendrimers, gold nanoparticles, organic dye, and oppositely charged proteins were also utilized as mediators.[3n–p] Another popular approach for constructing a nanostructure is to engineer the surface of protein cage nanoparticles by chemically and/or genetically adding interacting moieties and functional molecules and use their complimentary interactions. The biotin/streptavidin binding pair has primarily been utilized in nanostructure constructions with cowpea mosaic virus (CPMV), CCMV, and ferritin.[3b–f] Electrostatic and metal/ligand interactions were also utilized by inserting charged peptides or attaching metal-binding ligands for P22 virus–like particles and lumazine synthase.[3g,h,l,m,4] These approaches, however, often result in improper folding and aggregation of the fusion proteins, especially in protein cage nanoparticles, probably because the self-assembly process of large assembles might be interfered by the fused proteins.[5] For these reasons, the functional moieties introduced to the protein cage nanoparticles were often limited to short peptides or small domains, which limits the construction of functional nanostructures using protein cage nanoparticle–based functional building blocks.

H. Choi, B. Choi, H. Kim, Prof. S. Kang
Department of Biological Sciences
School of Life Sciences
Ulsan National Institute of Science and Technology (UNIST)
Ulsan 44919, South Korea
E-mail: sabsab7@unist.ac.kr
G. J. Kim, H. Kim, Prof. H. S. Jung
Department of Biochemistry
College of Natural Sciences
Kangwon National University
1, Kangwondaehak-gil, Chuncheon-si, Gangwon-do 24341, South Korea
The ORCID identification number(s) for the author(s) of this article can be found under https://doi.org/10.1002/smll.201801488.

DOI: 10.1002/smll.201801488

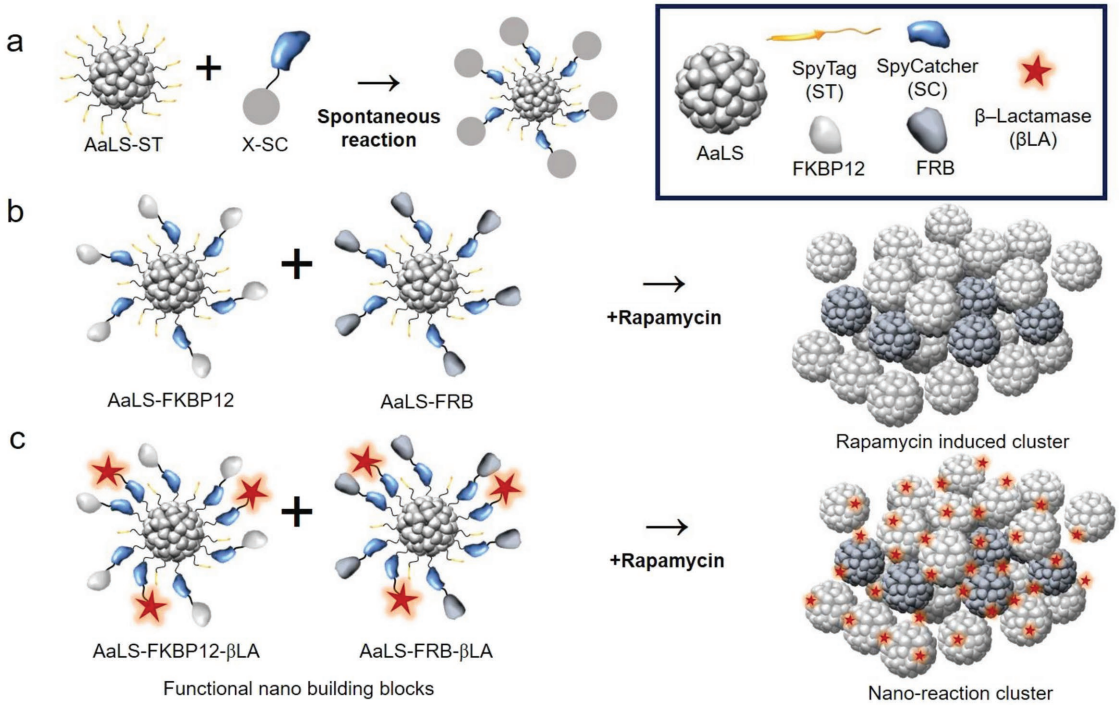

Figure 1. Schematic representation of the AaLS protein cage nanobuilding blocks and formation of the clusters. a) Polyvalent display of the functional proteins on the AaLS protein cage nanoparticles using the SpyTag/SpyCatcher protein ligation system. Reaction cluster formations of nanobuilding blocks b) without or c) with enzymes.

To circumvent these issues, we used a SpyTag/SpyCatcher (ST/SC) bacterial glue system to attach various functional proteins onto protein cage nanoparticles. The ST/SC bacterial glue system is a recently developed protein ligation system. The 15 kDa SC protein recognizes the 13 amino acid ST peptide spontaneously forming an irreversible isopeptide covalent bond, and each ST and SC can be genetically fused to many different types of proteins without significantly altering the function of the fused proteins.[6] Two individual functional proteins can be independently expressed and covalently ligated together to have multiple functions.[6b] Efficient displays of various antigenic proteins and domains on virus-like particles (VLPs) have been demonstrated.[7] The highly symmetric polyvalent nature of protein cage nanoparticles may allow efficient displays of multiple different functional proteins simultaneously on a single protein cage nanoparticle exhibiting multifunctions.

Here, we utilized lumazine synthase as a template protein cage nanoparticle due to its mechanical robustness and functional plasticity. Lumazine synthase we used was originally derived from the open reading frame specifying the putative 6,7-dimethyl-8-ribityl lumazine synthase of the hyperthermophile *Aquifex aeolicus* (AaLS) and consists of 60 identical subunits that self-assemble to form a hollow icosahedral capsid architecture (T = 1 state) having exterior and interior diameters of 15.4 and 9 nm, respectively.[8] AaLS is an enzyme that is involved in riboflavin biosynthesis by catalyzing its penultimate step and encapsulating riboflavin synthase forming the lumazine synthase/riboflavin synthase complex.[9] AaLS has been widely engineered to encapsulate cargo proteins and displays a variety of ligands. Engineering of the interior surface and/or interface of AaLS with negatively charged amino acids resulted in the formation of larger protein cage nanoparticle and allowed for efficient encapsulation of various cargo proteins.[10] Recently, AaLS was permuted creating new termini on the interior to form different tubular and spherical assemblies which allowed for effective modification of the interior surface to encapsulate guest proteins or RNA.[11] The interior cavity of AaLS was also used as a size-constraint nanoreactor to crystalize inorganic nanomaterials.[12] Target-binding ligands, contrast agents, and metal-binding ligands were also successfully displayed on the surface of AaLS through both genetic and chemical modifications.[3h,13]

In this study, we genetically engineered AaLS protein cage nanoparticles and developed functional nanobuilding blocks by polyvalently displaying multiple functional proteins on the AaLS protein cage nanoparticles utilizing the ST/SC bacterial glue system (**Figure 1**). Dual-functionalized nanobuilding blocks were further constructed by ligating both the binding ligands and enzymes together on a single AaLS protein cage nanoparticle. Stable 3D nanoreaction cluster formations were attempted with them in LbL configuration (Figure 1). Post-translational attachment of functional proteins to the robust and polyvalent protein cage nanoparticles may make it possible to display multiple copies of large functional proteins as well as two different types of functional proteins simultaneously on a single protein cage nanoparticle.

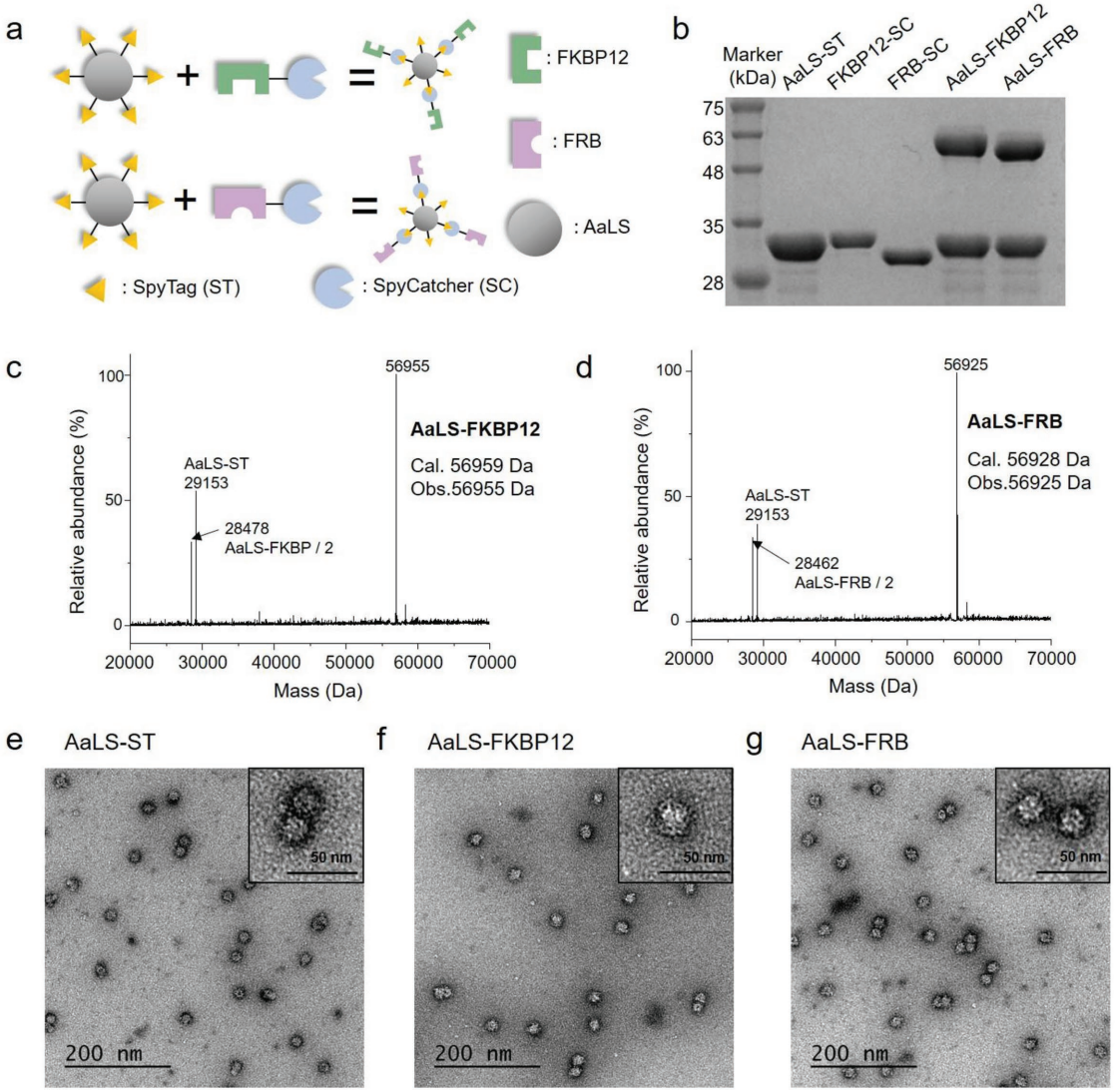

Figure 2. Construction and characterization of protein cage nanobuilding blocks. a) Illustration of reactions of AaLS–ST with either FKBP12–SC or FRB–SC to construct AaLS–FKBP12 or AaLS–FRB protein cage nanobuilding blocks. b) SDS-PAGE analyses of the individual proteins and their reaction resultants. c) Mass spectrometric analyses of the reaction resultants from AaLS–ST and FKBP12–SC. d) Mass spectrometric analysis of the reaction resultants from AaLS–ST and FRB–SC. Calculated and observed molecular masses are indicated. e) Transmission electron microscope images of AaLS–ST and the reaction resultants from f) AaLS–ST and FKBP12–SC, g) AaLS–ST and FRB–SC.

2. Result and Discussion

2.1. Construction of Protein Cage Nanoparticle–Based Building Blocks by the SpyTag/SpyCatcher Protein Ligation System

The ST/SC protein ligation system was utilized to construct protein cage nanobuilding blocks. To construct protein cage templates, the ST peptide with extra linker residues (GSGGAHIVMVDAYKPTK) was genetically introduced to the C-terminus of AaLS (AaLS–ST) where it is to be exposed to the surface (**Figure 2**a).[13c] Since an AaLS is composed of 60 copies of an identical subunit, each AaLS would display 60 ST peptides on its surface. Its ligation partner, the SC protein, was genetically fused with either a FKBP12 or FRB monomer to generate FKBP12–SpyCatcher (FKBP12–SC) or FRB–SpyCatcher (FRB–SC) (Figure 2a) which can form a stable FKBP12/FRB heterodimer upon addition of rapamycin. However, it is known that neither FKBP12 nor FRB itself form rapamycin-mediated homodimers because they do not share rapamycin-binding sites.[14] All three proteins have a hexa-histidine tag at the N-termini and were independently overexpressed in a bacterial system and simply purified with immobilized metal affinity chromatography (IMAC, nickel-nitrilotriacetic acid (Ni-NTA) agarose column). We obtained highly pure proteins (>98%) and verified the molecular masses of each protein with mass spectrometry (Figure S1, Supporting Information). Concentrations of each purified protein were determined with a bicinchoninic acid (BCA) protein assay.

To generate the basic building blocks (Figure 2a), AaLS–STs were mixed with either FKBP12–SC or FRB–SC. Covalent

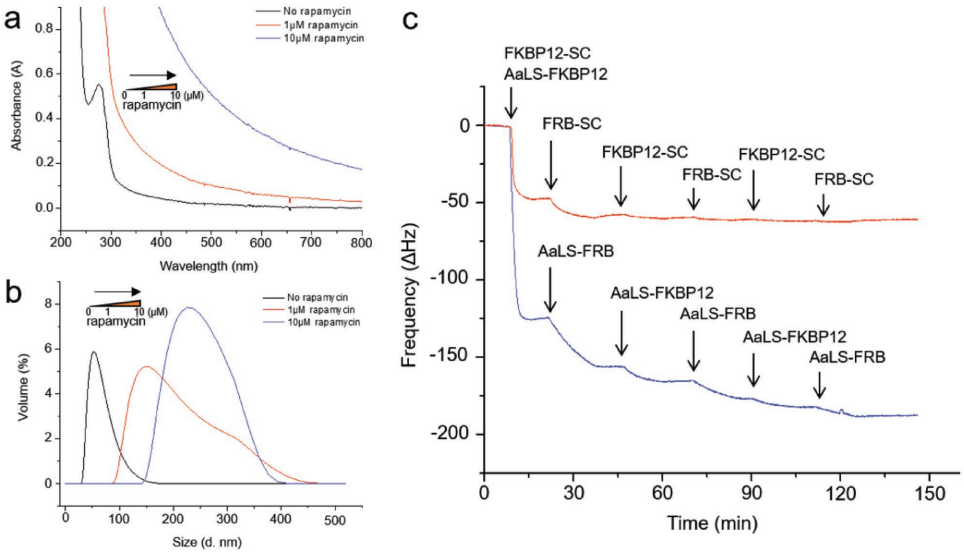

Figure 3. Cluster and LbL formations of protein cage nanobuilding blocks using rapamycin-induced FKBP12/FRB dimerization. a) Spectrophotometric and b) dynamic light scattering analyses of the reaction resultant from AaLS–FKBP12 and AaLS–FRB mixtures following rapamycin treatment (0, 1×10^{-6}, and 10×10^{-6} M). c) QCM resonance frequency changes by alternately introducing two complementary proteins (red, FKBP12–SC and FRB–SC; blue, AaLS–FKBP12 and AaLS–FRB).

ligations between the subunits of AaLS–ST and either FKBP12–SC or FRB–SC were almost complete in 20 min, and almost all of the subunits of the AaLS–ST were ligated with SC-fused proteins without altering cage architecture (Figure S2, Supporting Information). To save rooms for additional functionalizations, we treated the AaLS–ST with a half molar concentration of either FKBP12–SC or FRB–SC and analyzed them with sodium dodecyl sulfate polyacrylamide gel electrophoresis (SDS-PAGE) and mass spectrometry (MS). While each protein migrated to the estimated mass position on SDS-PAGE, the reaction mixtures exhibited two distinctly migrated bands which corresponded to the molecular masses of either the unreacted subunit of AaLS–ST (lower bands) or the sum of the masses of the AaLS–ST subunit and the SC-fused proteins (FKBP12–SC or FRB–SC) (Figure 2b). Mass spectrometric analyses confirmed covalent bond formation between AaLS–ST and the SC-fused proteins (Figure 2c). The calculated mass values of ligation resultants were the sum of the molecular masses of the ligated partner proteins and 18 Da subtraction resulted from the dehydration reaction of the isopeptide bond formation.[6a] Molecular masses of unreacted AaLS–ST subunit (observed mass value: 29 153.0 Da, calculated mass value: 29 153.6 Da) and either the FKBP12–SC-ligated AaLS–ST subunit (AaLS–FKBP12 subunit, observed: 56 955.0 Da, calculated: 56 958.3 Da) or the FRB–SC-ligated AaLS–ST subunit (AaLS–FRB subunit, observed: 56 925.0 Da, calculated: 56 927.3 Da) were measured simultaneously in reaction mixtures, and all the measured values corresponded well to the calculated values (Figure 2c). Additional mass peaks (indicated with ↙) from deconvoluted mass data besides those of the two main proteins were multiplied or divided values of the two main peaks which are harmonic artifacts caused by the broad MaxEnt1 output range.[15] The protein cage architectures of AaLS–FKBP12 and AaLS–FRB upon ligation were confirmed with transmission electron microscope (TEM) images, showing their spherical morphology with a uniform size distribution (Figure 2e–g). AaLS–FKBP12 and AaLS–FRB were eluted slightly earlier than AaLS–ST in size exclusion chromatography (SEC, Figure S3a,b, Supporting Information) and exhibited slightly larger hydrodynamic diameters (36.5 and 35.3 nm, respectively) than AaLS–ST (27.5 nm) in dynamic light scattering analyses (DLS, Figure S3c,d, Supporting Information) probably due to covalent display of either FKBP12 or FRB on the surface of AaLS. These results indicated that the covalent displays of the proteins on the AaLS surface were successfully achieved using the ST/SC ligation system without significantly disturbing the protein cage architectures.

2.2. Cluster and Layer-by-Layer Formations of Protein Cage Nanoparticle–Based Building Blocks Using Rapamycin-Mediated FKBP12/FRB Dimerization

To test whether AaLS–FKBP12 and AaLS–FRB could assemble upon rapamycin treatment, we mixed the solutions of AaLS–FKBP12 and AaLS–FRB (final FKBP12 or FRB concentration of 6×10^{-6} M each). Next, we added various amounts of rapamycin and monitored them by spectrophotometry and DLS (**Figure 3**a,b). In the solution, the addition of rapamycin induced light scattering in a dose-dependent manner (Figure 3a), indicating that AaLS–FKBP12 and AaLS–FRB building blocks spontaneously formed rapamycin-mediated large clusters. DLS data also showed sequential size increases following the addition of rapamycin (Figure 3b), consistent with the spectrophotometric measurements.

Cluster formation with AaLS–FKBP12 and AaLS–FRB building blocks in the solution, however, ultimately resulted in either heterogeneous clustering or uncontrolled aggregation of the protein building blocks. To achieve better assembly control and obtain a more ordered nanostructure, we attempted to build a LbL nanostructure on a 2D surface by alternately

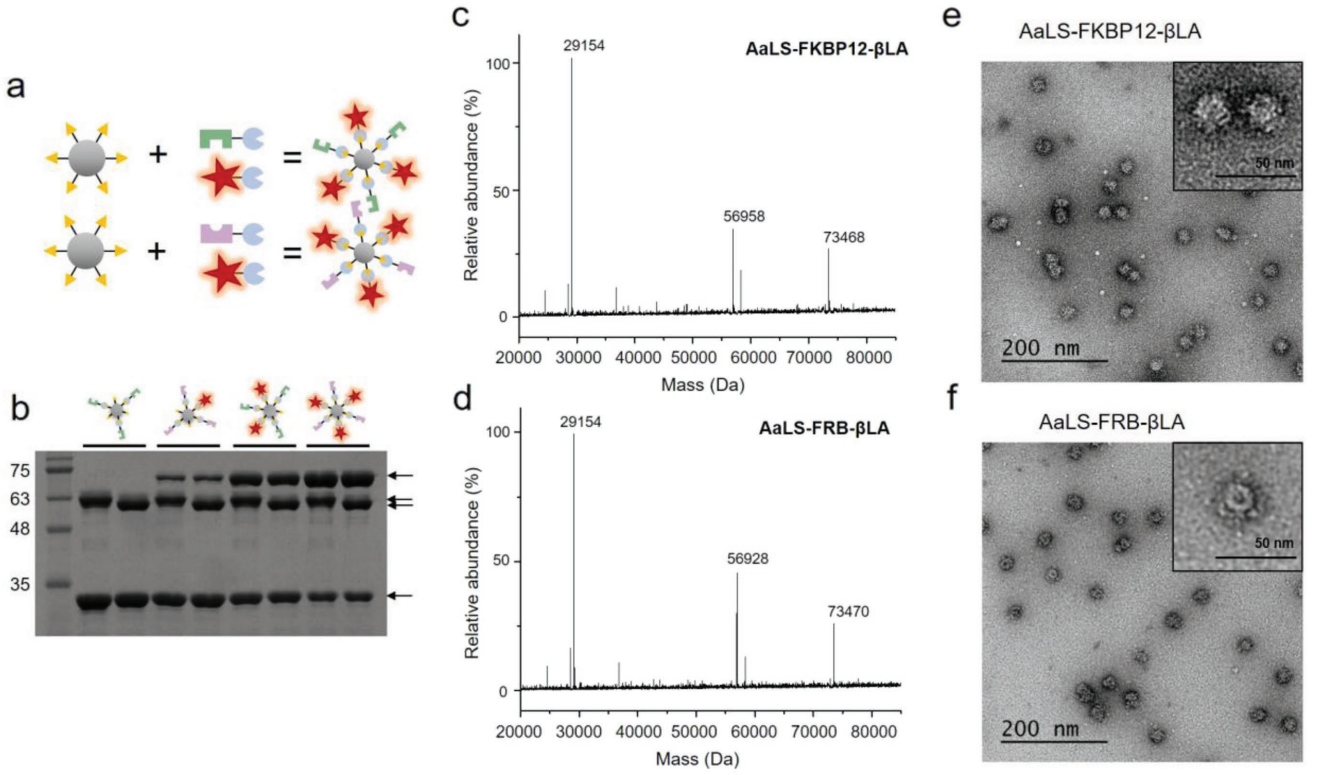

Figure 4. Construction and characterization of enzyme-ligated protein cage nanobuilding blocks. a) Illustration of reactions of AaLS–ST and SC proteins to construct AaLS–FKBP12–βLA and AaLS–FRB–βLA protein cage nanobuilding blocks. b) SDS-PAGE analyses of the reaction resultants from AaLS–ST and FKBP12–SC or FRB–SC with various amounts of βLA–SC. c) Mass spectrometric analysis of the reaction resultants from AaLS–ST, FKBP12–SC, and βLA–SC. d) Mass spectrometric analysis of the reaction resultants from AaLS–ST, FRB–SC, and βLA–SC. e) Transmission electron microscope imaging of the reaction resultants from AaLS–ST, FKBP12–SC, and βLA–SC. f) Transmission electron microscope images of the reaction resultants from AaLS–ST, FRB–SC, and βLA–SC.

depositing two complementary building blocks (AaLS–FKBP12 and AaLS–FRB) with the mediator rapamycin. LbL formation of those building blocks was assessed with quartz crystal microbalance (QCM) (Figure 3c). As the AaLS–FKBP and AaLS–FRB were alternately introduced to the QCM gold chip channel with rapamycin, the resonance frequency signals decreased stepwise. The first drastic reductions of frequency were observed upon introductions of either monomeric FKBP12–SC (red line) or AaLS–FKBP12 (blue line) at 10 min due to the simple adsorption of those proteins on to the gold chip sensor, forming a stable first layer (Figure 3c). Since AaLS–FKBP12 is much larger and heavier than monomeric FKBP12–SC, the deposition of AaLS–FKBP12 on the sensor chip surface led to a much larger reduction of frequency (Figure 3c). Subsequently, each complementary component, either monomeric FRB–SC or AaLS–FRB, was introduced to each channel with rapamycin and the corresponding frequency reductions were recorded (Figure 3c). Next frequency reductions were due to the binding of each complementary component induced by the rapamycin-mediated interaction between FKBP12 and FRB, which were either by alone (FKBP12–SC/FRB–SC) or displayed on the AaLS surface (AaLS–FKBP12/AaLS–FRB). Continuous stepwise reductions of frequency were observed upon the alternate introductions of AaLS–FKBP12/AaLS–FRB with rapamycin (Figure 3c). In contrast, the stepwise reduction of frequency stopped with the first introduction of monomeric FRB–SC (red line). This is likely due to only one binding site in each monomer, which was capped in the second layer to be completed. These results indicate that AaLS–FKBP and AaLS–FRB were alternately deposited on the 2D surface mediated by rapamycin to form stable LbL structure.

2.3. Construction of the Enzyme-Ligated Protein Cage Nanobuilding Blocks

Since both AaLS–FKBP12 and AaLS–FRB had 30–35 unreacted STs per particle on the surface, we additionally ligated β-lactamase–SC (βLA–SC) to them to make functional nanobuilding blocks (**Figure 4**a). SDS-PAGE analyses of the reactions between βLA–SC and protein cage nanobuilding blocks (AaLS–FKBP12 or AaLS–FRB) showed three distinct bands corresponding to the subunit masses of β-lactamase-conjugated AaLS (AaLS–βLA), AaLS–FKBP12 (or AaLS–FRB), and unreacted AaLS–ST from top to the bottom (Figure 4b). The desired ratios of two different surface proteins (FKBP12 or FRB vs βLA) were achieved by controlling the input amounts of FKBP12–SC (or FRB–SC) and βLA–SC relative to the AaLS–ST subunit (40% vs 0%, 10%, 30%, or 50%; Figure 4b). Mass analyses of the reaction resultants confirmed that molecular

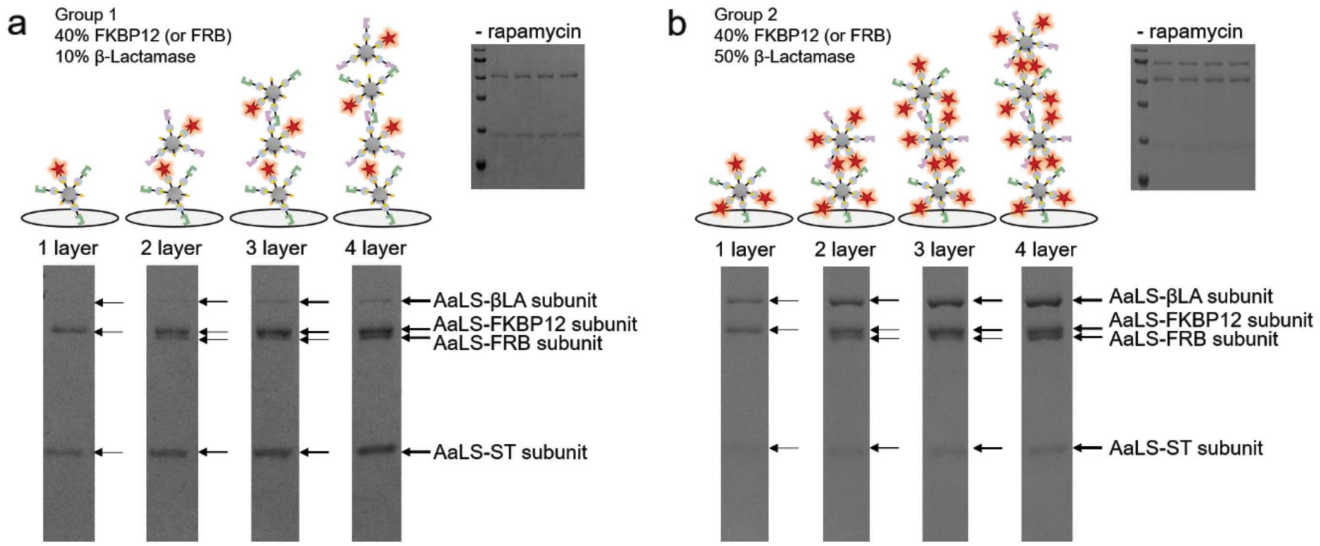

Figure 5. Formation of nanoreaction clusters with the dual-functional protein cage nanobuilding blocks in 96-well plates. Schematic representations and SDS-PAGE analyses of the LbL assemblies constructed by a) group 1 (40% of either FKBP12 or FRB and 10% of βLA) and b) group 2 (40% of either FKBP12 or FRB and 50% of βLA) nanobuilding blocks with rapamycin. Insets are SDS-PAGE results of LbL assemblies without rapamycin.

masses of three different species we observed in SDS-PAGE analyses (Figure 4b) corresponded well with the calculated molecular masses of AaLS–ST, AaLS–FKBP12 (or AaLS–FRB), and AaLS–FKBP12–βLA (or AaLS–FRB–βLA) subunits (Figure 4c,d and Figure S4 (Supporting Information)). DLS and SEC data revealed that additional attachment of βLA to the protein building blocks resulted in slight size increase (Figure S3, Supporting Information). The TEM images showed the spherical protein cage architectures of dual-functionalized protein building blocks with uniform size distribution (Figure 4e,f). These data indicate that βLA–SCs were successfully ligated onto the surface of AaLS–FKBP12 or AaLS–FRB, making dual-functional (enzyme activity and binding capability) protein cage nanobuilding blocks (Figure 4a).

2.4. Nanoreaction Cluster Formation of the Enzyme-Ligated Protein Cage Nanoparticle–Based Building Blocks in LbL Configuration

To evaluate the LbL formation capability of enzyme-ligated protein building blocks (AaLS–FKBP12–βLA and AaLS–FRB–βLA), we applied the same QCM technique and observed stepwise frequency reduction patterns with AaLS–FKBP12–βLA and AaLS–FRB–βLA, similar to the previous QCM data regardless of the conjugation of βLA (Figure S5, Supporting Information).

To investigate the enzymatic activity in the reaction clusters depending on their configuration, we utilized a high-binding 96-well enzyme-linked immunosorbent assay (ELISA) plate as a platform for LbL deposition. We utilized two different groups of protein cage nanobuilding blocks which are ligated with different amounts of βLA (6 vs 30 units per building block) to investigate the effects of the amount of enzyme and the level of depositions on the enzymatic activity. While group 1 was composed of 40% of either FKBP12 or FRB (≈24 subunits) and 10% of βLA (6 subunits), group 2 consisted of 40% of either FKBP12 or FRB (≈24 subunits) and 50% of βLA (30 subunits) (Figure 4b). The first layer was formed by a physical absorption of the βLA-ligated protein cage nanobuilding blocks to the 96-well plate and, complementary counterparts were alternately added with rapamycin to construct nanoreaction clusters in LbL configuration up to four layers as previously described. We washed the wells extensively with buffer after each deposition. Prior to evaluating the enzymatic activity, deposited proteins were detached using SDS and analyzed with SDS-PAGE for qualification and quantification (**Figure 5** and Figure S6 (Supporting Information)). As the layers accumulated, all protein bands on the SDS-PAGE appeared and their intensity increased, suggesting that the LbL structure was successfully built up through rapamycin-mediated FKBP12/FRB dimerization in the 96-well plate. In particular, the amounts of AaLS–βLA subunits gradually increased as the layers accumulated in both group 1 and group 2 (Figure S6b, Supporting Information). Since each AaLS particle in group 2 contained much more enzymes, total amounts of enzymes in group 1 were significantly lower than those of group 2 (Figure 5 and Figure S6b (Supporting Information)). In contrast, we did not observe any significant increase in band intensity without rapamycin (Figure 5, insets).

To evaluate the enzymatic activities of constructed nanoreaction clusters, we prepared eight different nanoreaction clusters which have one to four layers of either group 1 (40% FKBP12 or FRB + 10% of βLA) or group 2 (40% FKBP12 or FRB + 50% of βLA) building blocks. We treated them with nitrocefin which is a substrate of βLA undergoing color change from yellow to red upon enzymatic conversion and monitored the OD486 for 45 min (**Figure 6**). Enzymatic conversions of nitrocefin occurred more in the single layer–built complexes with group 2 compared with group 1 (Figure 6 and Figure S7 (Supporting Information), black squares) likely due to greater numbers of βLA on the same number of building blocks attached to the surface of the well (50% vs 10%, Figure S6b, Supporting Information). As the numbers of layers increased, enzymatic conversions of

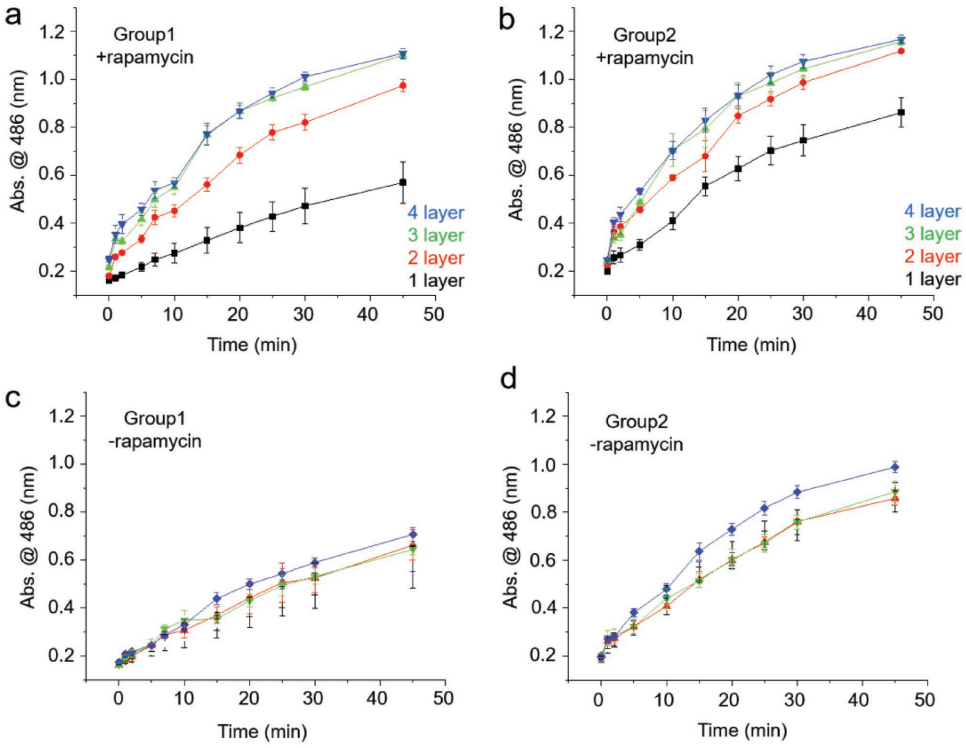

Figure 6. Enzymatic activities of nanoreaction clusters. Enzyme conversions of nitrocefin were monitored by measuring the OD486 with a microplate reader. a) LbL assemblies constructed with group 1 nanobuilding blocks and rapamycin. b) LbL assemblies constructed with group 2 nanobuilding blocks and rapamycin. c) LbL assemblies constructed with group 1 nanobuilding blocks only. d) LbL assemblies constructed with group 2 nanobuilding blocks only. Black squares (single layer), red circles (double layer), green triangles (triple layer), and blue diamonds (quadruple layer).

nitrocefin increased in LbL structures built with both group 1 and group 2 building blocks (Figure 6a,b). Cumulative 3D deposits of AaLS–βLA may increase addressable numbers of enzymes in the 3D space, resulting in increased enzymatic conversions of nitrocefin. Interestingly, we observed better enzymatic conversion from nitrocefin with double-layered clusters of group 1 compared with single layer of group 2, although the total amount of βLA in the single layer of group 2 (0.862 pmol) was significantly larger than that of the double-layered cluster of group 1 (0.471 pmol) based on the quantity using SDS-PAGE (Figure 5 and Figure S6b (Supporting Information)). These results suggest that the 3D array of enzymes allows better accessibility of substrates, resulting in better performance. Nanoreaction cluster formation attempts without rapamycin did not show any significant increase in substrate conversion over single layer to quadruple layers (Figure 6c,d), suggesting that there is no significant additional layer formation beyond the single layer or detachment of first layer (Figure 5, insets). Although we observed greater absorbance in the more layered nanoreaction clusters in both group 1 and group 2, we did not observe linear absorbance increment according to the increase of layers (Figure 6a,b). The largest absorbance increments were observed between single- and double-layered clusters, and absorbance enhancement decreased as the more layers were added in both group 1 and group 2. While we only observed a slight increase in absorbance between triple- and quadruple-layered clusters in both group 1 and group 2 (Figure 6a,b), the values of initial reaction rate per enzyme in multilayered (2 to 4) clusters were similar to each other in group 1 or slightly decreased as the more layers were added in group 2 (Figure S6c, Supporting Information). However, the values of initial reaction rate per enzyme in multilayered (2 to 4) clusters of group 1 were significantly higher than those in multilayered (2 to 4) clusters of group 2 (Figure S6c, Supporting Information). Building blocks, particularly densely decorated with enzymes, may be tightly packed and networked together through multivalent rapamycin-mediated FKBP12/FRB interactions, and the substrates may have trouble accessing deep into the layered clusters with more than triple layers. However, it is also possible that the total enzymatic rates of highly packed enzymes saturate at some point and the increased activity allowed by adding one more active site is negligible because a substrate that reaches any depth in the clusters is likely to collide with many other enzyme sites before escaping anyway. We cannot rule out any of above possibilities and further studies with regularly packed lattice of protein cage nanoparticles may give better understanding.

3. Conclusion

In summary, ST was genetically fused to the surface of AaLS, and SC was fused to βLA and two complementary protein ligands, FKBP12 and FRB, independently. Dual-functional protein cage nanobuilding blocks, AaLS–FKBP12–βLA and AaLS–FRB–βLA, were successfully generated by the simultaneous ligation of two different SC-fused functional proteins on an

AaLS protein cage nanoparticle using the ST/SC bacterial glue system. Covalent protein ligations were confirmed by SDS-PAGE and MS analyses, and their intact cage structures and surface display of proteins were verified with TEM, DLS, and SEC. AaLS–FKBP12–βLA and AaLS–FRB–βLA were alternately deposited on the 2D surface mediated by rapamycin to form 3D nanoreaction clusters in a stable layer-by-layer configuration, and they exhibited superior total enzymatic activity compared with a single-layered 2D array. The post-translational protein ligation method made it possible to display large functional proteins polyvalently on a single protein cage nanoparticle and two different types of functional proteins simultaneously on a single protein cage nanoparticle in a controlled way. The approach we described here can be applied to the other protein cage nanoparticles, enzymes, and functional proteins and may provide new opportunities for fabricating novel functional nanostructures to develop target-specific delivery nanoplatforms and nanostructured biosensors.

4. Experimental Section

Molecular Cloning, Protein Expression, and Purification: Original genes of SC and βLA were a gift from Mark Howarth (Addgene plasmid #52656).[16] Original genes of FKBP12 and FRB were kindly provided by Prof. Hyun-Woo Rhee. AaLS–ST, FKBP12–SC, and FRB–SC genes were cloned into the pETDuet-1 vector (Amp^R). The βLA–SC gene was cloned into the pET-30b vector (Kan^R) due to the β-lactamase cleaving β-lactam ring of ampicillin. Each vector was transformed into competent *Escherichia coli* strain BL21 (DE3) and candidate colonies were tested for expression and verified by DNA sequencing. Cells were grown at 37 °C and induced with 500×10^{-6} M isopropyl β-D-1-thiogalactopyranoside (IPTG) at an optical density (OD) 600 of 0.5 and then further cultured overnight at 30 °C. For monomeric proteins, cells were harvested and lysed with lysozyme followed by sonication, and cellular debris was removed by centrifugation (15 000 × *g*, 1 h). Proteins in the cell lysate were purified by fast protein liquid chromatography (FPLC) using IMAC (Ni–NTA agarose column). The AaLS–ST purification process required additional heating (65 °C, 10 min) and centrifugation (15 000 × *g*, 30 min) in between the sonication and FPLC steps.

Mass Spectrometry: The molecular masses of genetically and post-translationally modified proteins were analyzed using an electrospray ionization time-of-flight (ESI-TOF) mass spectrometer (Xevo G2 TOF, waters) interfaced with a water UPLC and autosampler. Samples were loaded onto a MassPREP Micro-desalting column (Waters) and eluted with a gradient of 5–95% v/v acetonitrile containing 0.1% formic acid at a flow rate of 500 µL min^{-1}. ESI generally produces a series of multiply charged ions, and the charges are distributed as a continuous series with a Gaussian intensity distribution. The molecular masses of each species can be determined from the charges and the observed mass-to-charge (*m*/*z*) ratio values. Mass spectra were acquired in the range of *m*/*z* 500–3000 and deconvoluted using MaxEnt1 from MassLynx version 4.1 to obtain the average mass from multiple charge-state distributions. For clarity, only deconvoluted masses were presented.

DLS: DLS was performed using a Malvern zetasizer with a disposable rectangular polystyrene cuvette. Each sample solution was prepared at ≈1 mg mL^{-1} in phosphate buffered saline (PBS) and adjusted to room temperature before being introduced to the instrument. The system was operated in 25 °C, and scattered light was measured at a 90° angle with the projected light. The samples were equilibrated for 2 min before being measured in triplicate.

QCM: QCM was performed with Q-Sense E4 and standard gold QCM sensors (Q-sense, Sweden). The system was operated at a flow rate of 0.6 mL min^{-1} with the multichannel peristalsis pump at room temperature. Each sample solution was introduced into the measurement chamber through the pump and continuously measured until the samples became saturated. All the samples were prepared at a concentration of 100 µg mL^{-1} in PBS with 1×10^{-6} M of rapamycin. Resonance frequencies were measured simultaneously at seven harmonics (5, 15, 25, 35, 45, 55, and 65 MHz). For clarity, only the normalized frequency of the third overtone was shown.

LbL Formation of Nanobuilding Blocks in 96-Well Plates and an Enzyme Assay: Each protein sample was prepared at a concentration of 0.5 mg mL^{-1} in PBS containing 10×10^{-6} M rapamycin. The LbL formation experiment was conducted in Immuno MicroWell 96-well plates (Nunc Maxisorp, flat-bottom, 400 µL). First sample (AaLS–FKBP12–βLA, 100 µL each) was loaded in the well and incubated at 4 °C overnight to immobilize the sample on the surface of the plate through physical adsorption to form first single layer. The next day, each well was washed three times with PBS then the complementary nanobuilding block sample (100 µL each) was loaded into the well and incubated at room temperature on the orbital shaker (120 rpm) for 1 h. This process was repeated to construct triple and quadruple layers. Finally, each well was washed five times with PBS for 10 min on an orbital shaker (120 rpm). The actual amounts of βLA in the LbL was determined by measuring band intensities in SDS-PAGE analyses of each layer and comparing with a standard curve which was established with SDS-PAGE band intensity analyses with known amounts of AaLS–βLA. Nitrocefin (Cayman Chemical) was prepared in 0.5×10^{-3} M 0.1 M phosphate buffer pH 7.0, and 100 µL of the solution was loaded into each well. The OD486 of each well was monitored in various time points from 0 to 45 min with a microplate reader, SpectraMAX 190 (Molecular Devices). All the experiments were repeated four times and plotted with error.

Supporting Information

Supporting Information is available from the Wiley Online Library or from the author.

Acknowledgements

This work was supported by the National Research Foundation of Korea (NRF) grant (Nos. NRF- 2016R1D1A1B03932580 and 2018R1A6A1A03025810) funded by the Korean government. The electron microscopy research was supported by Next-Generation BioGreen 21 Program (SSAC, PJ013273042018).

Conflict of Interest

The authors declare no conflict of interest.

Keywords

bacterial superglue, layer-by-layer assembly, lumazine synthase, nanobuilding blocks, nanoclusters

Received: April 18, 2018
Revised: June 8, 2018
Published online:

[1] a) Z. Nie, A. Petukhova, E. Kumacheva, *Nat. Nanotechnol.* **2010**, *5*, 15; b) J. He, Y. Liu, T. Babu, Z. Wei, Z. Nie, *J. Am. Chem. Soc.* **2012**, *134*, 11342; c) C. Schmidtke, R. Eggers, R. Zierold, A. Feld, H. Kloust, C. Wolter, J. Ostermann, J. P. Merkl, T. Schotten, K. Nielsch, H. Weller, *Langmuir* **2014**, *30*, 11190; d) D. Men, T. T. Zhang,

L. W. Hou, J. Zhou, Z. P. Zhang, Y. Y. Shi, J. L. Zhang, Z. Q. Cui, J. Y. Deng, D. B. Wang, X. E. Zhang, *ACS Nano* **2015**, *9*, 10852.

[2] a) L. Q. Wu, G. F. Payne, *Trends Biotechnol.* **2004**, *22*, 593; b) P. J. Yoo, K. T. Nam, J. Qi, S. K. Lee, J. Park, A. M. Belcher, P. T. Hammond, *Nat. Mater.* **2006**, *5*, 234; c) M. S. Gudiksen, L. J. Lauhon, J. Wang, D. C. Smith, C. M. Lieber, *Nature* **2002**, *415*, 617; d) R. Shenhar, V. M. Rotello, *Acc. Chem. Res.* **2003**, *36*, 549; e) Y. Hu, H. O. Churchill, D. J. Reilly, J. Xiang, C. M. Lieber, C. M. Marcus, *Nat. Nanotechnol.* **2007**, *2*, 622; f) F. Liu, K. Huang, Q. Wu, S. Dai, *Adv. Mater.* **2017**, *29*, 1700445; g) B. D. B. Tiu, R. B. Pernites, S. B. Tin, R. C. Advincula, *Colloids Surf., A* **2016**, *495*, 149; h) Z. Chen, C. Zhang, X. Li, H. Ma, C. Wan, K. Li, Y. Lin, *Biosens. Bioelectron.* **2015**, *65*, 232; i) A. B. Nandiyanto, A. Suhendi, O. Arutanti, T. Ogi, K. Okuyama, *Langmuir* **2013**, *29*, 6262.

[3] a) Y. Ko, S. W. Ryu, J. Cho, *Appl. Surf. Sci.* **2016**, *368*, 36; b) Y. J. Kang, M. Uchida, H. H. Shin, T. Douglas, S. Kang, *Soft Matter* **2011**, *7*, 11078; c) P. A. Suci, M. T. Klem, F. T. Arce, T. Douglas, M. Young, *Langmuir* **2006**, *22*, 8891; d) N. F. Steinmetz, G. Calder, G. P. Lomonossoff, D. J. Evans, *Langmuir* **2006**, *22*, 10032; e) N. F. Steinmetz, E. Bock, R. P. Richter, J. P. Spatz, G. P. Lomonossoff, D. J. Evans, *Biomacromolecules* **2008**, *9*, 456; f) P. Suci, M. T. Klem, M. Young, T. Douglas, *Soft Matter* **2008**, *4*, 2519; g) A. Servid, P. Jordan, A. O'Neil, P. Prevelige, T. Douglas, *Biomacromolecules* **2013**, *14*, 2989; h) H. Moon, W. G. Kim, S. Lim, Y. J. Kang, H. H. Shin, H. Ko, S. Y. Hong, S. Kang, *J. Mater. Chem. B* **2013**, *1*, 4504; i) C. L. Cheung, J. A. Camarero, B. W. Woods, T. Lin, J. E. Johnson, J. J. De Yoreo, *J. Am. Chem. Soc.* **2003**, *125*, 6848; j) R. A. McMillan, J. Howard, N. J. Zaluzec, H. K. Kagawa, R. Mogul, Y. F. Li, C. D. Paavola, J. D. Trent, *J. Am. Chem. Soc.* **2005**, *127*, 2800; k) A. K. Udit, S. Brown, M. M. Baksh, M. G. Finn, *J. Inorg. Biochem.* **2008**, *102*, 2142; l) M. Uchida, K. McCoy, M. Fukuto, L. Yang, H. Yoshimura, H. M. Miettinen, B. LaFrance, D. P. Patterson, B. Schwarz, J. A. Karty, P. E. PreveligeJr., B. Lee, T. Douglas, *ACS Nano* **2018**, *12*, 942; m) V. Liljestrom, J. Seitsonen, M. A. Kostiainen, *ACS Nano* **2015**, *9*, 11278; n) V. Liljestrom, J. Mikkila, M. A. Kostiainen, *Nat. Commun.* **2014**, *5*, 4445; o) M. A. Kostiainen, P. Hiekkataipale, A. Laiho, V. Lemieux, J. Seitsonen, J. Ruokolainen, P. Ceci, *Nat. Nanotechnol.* **2013**, *8*, 52; p) J. Mikkila, E. Anaya-Plaza, V. Liljestrom, J. R. Caston, T. Torres, L. Escosura Ade, M. A. Kostiainen, *ACS Nano* **2016**, *10*, 1565.

[4] a) M. A. Kostiainen, P. Ceci, M. Fornara, P. Hiekkataipale, O. Kasyutich, R. J. Nolte, J. J. Cornelissen, R. D. Desautels, J. van Lierop, *ACS Nano* **2011**, *5*, 6394; b) M. A. Kostiainen, O. Kasyutich, J. J. Cornelissen, R. J. Nolte, *Nat. Chem.* **2010**, *2*, 394.

[5] a) H. X. Zhou, *Acc. Chem. Res.* **2004**, *37*, 123; b) M. L. Smith, J. A. Lindbo, S. Dillard-Telm, P. M. Brosio, A. B. Lasnik, A. A. McCormick, L. V. Nguyen, K. E. Palmer, *Virology* **2006**, *348*, 475.

[6] a) B. Zakeri, J. O. Fierer, E. Celik, E. C. Chittock, U. Schwarz-Linek, V. T. Moy, M. Howarth, *Proc. Natl. Acad. Sci. USA* **2012**, *109*, E690; b) H. Moon, Y. Bae, H. Kim, S. Kang, *Chem. Commun.* **2016**, *52*, 14051.

[7] a) S. Thrane, C. M. Janitzek, S. Matondo, M. Resende, T. Gustavsson, W. A. de Jongh, S. Clemmensen, W. Roeffen, M. van de Vegte-Bolmer, G. J. van Gemert, R. Sauerwein, J. T. Schiller, M. A. Nielsen, T. G. Theander, A. Salanti, A. F. Sander, *J. Nanobiotechnol.* **2016**, *14*, 30; b) C. M. Janitzek, S. Matondo, S. Thrane, M. A. Nielsen, R. Kavishe, S. B. Mwakalinga, T. G. Theander, A. Salanti, A. F. Sander, *Malar. J.* **2016**, *15*, 545; c) K. D. Brune, D. B. Leneghan, I. J. Brian, A. S. Ishizuka, M. F. Bachmann, S. J. Draper, S. Biswas, M. Howarth, *Sci. Rep.* **2016**, *6*, 19234; d) D. B. Leneghan, K. Miura, I. J. Taylor, Y. Li, J. Jin, K. D. Brune, M. F. Bachmann, M. Howarth, C. A. Long, S. Biswas, *Sci. Rep.* **2017**, *7*, 3811.

[8] X. F. Zhang, W. Meining, M. Fischer, A. Bacher, R. Ladenstein, *J. Mol. Biol.* **2001**, *306*, 1099.

[9] a) X. Zhang, W. Meining, M. Cushman, I. Haase, M. Fischer, A. Bacher, R. Ladenstein, *J. Mol. Biol.* **2003**, *328*, 167; b) R. Ladenstein, M. Fischer, A. Bacher, *FEBS J.* **2013**, *280*, 2537; c) Y. Azuma, R. Zschoche, D. Hilvert, *J. Biol. Chem.* **2017**, *292*, 10321.

[10] a) E. Sasaki, D. Bohringer, M. van de Waterbeemd, M. Leibundgut, R. Zschoche, A. J. Heck, N. Ban, D. Hilvert, *Nat. Commun.* **2017**, *8*, 14663; b) F. P. Seebeck, K. J. Woycechowsky, W. Zhuang, J. P. Rabe, D. Hilvert, *J. Am. Chem. Soc.* **2006**, *128*, 4516; c) T. Beck, S. Tetter, M. Kunzle, D. Hilvert, *Angew. Chem., Int. Ed.* **2015**, *54*, 937; d) B. Worsdorfer, K. J. Woycechowsky, D. Hilvert, *Science* **2011**, *331*, 589; e) B. Worsdorfer, Z. Pianowski, D. Hilvert, *J. Am. Chem. Soc.* **2012**, *134*, 909; f) Y. Azuma, R. Zschoche, M. Tinzl, D. Hilvert, *Angew. Chem., Int. Ed.* **2016**, *55*, 1531; g) Y. Azuma, D. L. V. Bader, D. Hilvert, *J. Am. Chem. Soc.* **2018**, *140*, 860.

[11] a) Y. Azuma, M. Herger, D. Hilvert, *J. Am. Chem. Soc.* **2018**, *140*, 558; b) Y. Azuma, T. G. W. Edwardson, N. Terasaka, D. Hilvert, *J. Am. Chem. Soc.* **2018**, *140*, 566.

[12] W. Shenton, S. Mann, H. Colfen, A. Bacher, M. Fischer, *Angew. Chem., Int. Ed.* **2001**, *40*, 442.

[13] a) Y. Song, Y. J. Kang, H. Jung, H. Kim, S. Kang, H. J. Cho, *Sci. Rep.* **2015**, *5*, 15656; b) J. Min, S. Kim, J. Lee, S. Kang, *RSC Adv.* **2014**, *4*, 48596; c) H. Kim, Y. J. Kang, J. Min, H. Choi, S. Kang, *RSC Adv.* **2016**, *6*, 19208.

[14] a) J. Choi, J. Chen, S. L. Schreiber, J. Clardy, *Science* **1996**, *273*, 239; b) L. A. Banaszynski, C. W. Liu, T. J. Wandless, *J. Am. Chem. Soc.* **2005**, *127*, 4715.

[15] G. Sundqvist, M. Stenvall, H. Berglund, J. Ottosson, H. Brumer, *J. Chromatogr. B: Anal. Technol. Biomed. Life Sci.* **2007**, *852*, 188.

[16] C. Schoene, J. O. Fierer, S. P. Bennett, M. Howarth, *Angew. Chem., Int. Ed.* **2014**, *53*, 6101.